THE JOURNAL OF BIOLOGICAL CHEMISTRY VOL. 282, NO. 46, pp. 33572–33582, November 16, 2007

Kinetic Mechanism of Human dUTPase, an Essential Nucleotide Pyrophosphatase Enzyme*

Received for publication, July 30, 2007, and in revised form, September 7, 2007 Published, JBC Papers in Press, September 11, 2007, DOI 10.1074/jbc.M706230200

Judit Tóth[‡1], **Balázs Varga**[‡], **Mihály Kovács**[§], **András Málnási-Csizmadia**[§], **and Beáta G. Vértessy**[‡2]

From the [‡]*Institute of Enzymology, Biological Research Center, Hungarian Academy of Sciences, Karolina út 29, 1113 Budapest, Hungary and the* [§]*Eötvös Loránd University, Budapest, Hungary*

Human dUTPase is essential in controlling relative cellular levels of dTTP/dUTP, both of which can be incorporated into DNA. The nuclear isoform of the enzyme has been proposed as a promising novel target for anticancer chemotherapeutic strategies. The recently determined three-dimensional structure of this protein in complex with an isosteric substrate analogue allowed in-depth structural characterization of the active site. However, fundamental steps of the dUTPase enzymatic cycle have not yet been revealed. This knowledge is indispensable for a functional understanding of the molecular mechanism and can also contribute to the design of potential antagonists. Here we present detailed pre-steady-state and steady-state kinetic investigations using a single tryptophan fluorophore engineered into the active site of human dUTPase. This sensor allowed distinction of the apoenzyme, enzyme-substrate, and enzyme-product complexes. We show that the dUTP hydrolysis cycle consists of at least four distinct enzymatic steps: (i) fast substrate binding, (ii) isomerization of the enzyme-substrate complex into the catalytically competent conformation, (iii) a hydrolysis (chemical) step, and (iv) rapid, nonordered release of the products. Independent quenched-flow experiments indicate that the chemical step is the rate-limiting step of the enzymatic cycle. To follow the reaction in the quenched-flow, we devised a novel method to synthesize γ-^{32}P-labeled dUTP. We also determined by indicator-based rapid kinetic assays that proton release is concomitant with the rate-limiting hydrolysis step. Our results led to a quantitative kinetic model of the human dUTPase catalytic cycle and to direct assessment of relative flexibilities of the C-terminal arm, critical for enzyme activity, in the enzyme-ligand complexes along the reaction pathway.

dUTPase is the unique enzyme that specifically hydrolyzes the α-β pyrophosphate bond of dUTP to yield dUMP and PP_i (1). The enzyme is essential in maintaining DNA integrity in dividing cells (2, 3). Its activity is responsible for setting the physiological dUTP/dTTP concentration ratios (1:24) (4), thus preventing high rates of uracil incorporation into newly synthesized DNA. Although uracil in DNA is tolerated to a certain level by the base excision DNA repair mechanisms, higher levels of uracil in DNA trigger double-strand breaks and lead to cell death (5). Several lines of evidence show that up-regulated dUTPase is responsible for desensitizing tumors to drugs inhibiting the thymidylate synthase pathway, thus acting as an important survival factor for tumor cells (6, 7). Increased levels of the nuclear isoform of the enzyme correlate to worsened prognosis of several tumors, as revealed by detailed analysis of tissue samples (8, 9). dUTPase has therefore emerged as a high potential anticancer drug target, which possesses several additional, possibly advantageous features for drug design. Unlike most nucleotide-metabolizing enzymes, dUTPase is extremely specific to its substrate nucleotide, potentially allowing construction of substrate analogue antagonists with similarly high specificity. The nuclear isoform of the enzyme is under strict cell cycle control; its expression is mostly limited to rapidly dividing (including cancer) cells (10, 11). In addition to the fact that the enzyme is an important focus in biomedical research, dUTPase also serves as a model system for detailed analysis of enzyme-catalyzed nucleotide pyrophosphorolysis.

Current knowledge of the dUTPase mechanism is mainly based on three-dimensional structural approaches. Most dUTPases are homotrimers with a unique active site architecture, where all three monomers contribute to each of the three catalytic sites. High resolution crystal structures of the human (hDUT)[3] (12, 13) and other (14–18) dUTPases provided important mechanistic clues. The catalytic site is formed by five conserved motifs, four of which are contributed by two adjacent monomers. The fifth motif, positioned on the C-terminal arm, is usually provided by the third monomer. The C terminus, associated with an increased conformational freedom, was suggested to close upon the active site during the chemical step (12, 14, 19). Cleavage of the α-β pyrophosphate linkage is initiated by a nucleophilic attack from the catalytic water molecule coordinated by a conserved aspartate (Asp^{102} in the human enzyme) within the third motif accommodating the uracil and deoxyribose moieties of dUTP (16).

* This work was supported by Hungarian Scientific Research Fund Grant K68229, Howard Hughes Medical Institutes (HHMI) Grants 55005628 and 55000342, and a European Molecular Biology Organization (EMBO) long term postdoctoral fellowship (to J. T.); National Institutes of Health (NIH) Grant D43 TW006230 (1 R01 TW007241-01) funded by the Fogarty International Center and the NHLBI, NIH, an EMBO-HHMI startup grant, and the Bolyai Fellowship of the Hungarian Academy of Sciences (to M. K.); and grants from the Alexander von Humboldt Foundation and Varga József Foundation and Hungarian Economic Competitiveness Operative Programme Grants GVOP-3.2.1.-2004-05-0412/3.0, FP6 STREP 012127, and FP6 SPINE2c LSHG-CT-2006-031220. The costs of publication of this article were defrayed in part by the payment of page charges. This article must therefore be hereby marked "*advertisement*" in accordance with 18 U.S.C. Section 1734 solely to indicate this fact.

[1] To whom correspondence may be addressed. E-mail: tothj@enzim.hu.
[2] To whom correspondence may be addressed. E-mail: vertessy@enzim.hu.

[3] The abbreviations used are: hDUT, nuclear isoform of human dUTPase, His-tagged; dUPNPP, α,β-imido-dUTP; $hDUT^{W158}$, F158W mutant of nuclear isoform of human dUTPase, His-tagged; NATA, *N*-acetyl-L-tryptophanamide; NDPK, nucleoside triphosphate kinase.

Modern pharmacology demands knowledge of the precise mechanism of action of target enzymes. However, structural data have not yet been complemented by detailed solution kinetic studies for any eukaryotic dUTPase, possibly due to the lack of suitable optical signals reporting enzymatic events. Relying on proton escape during nucleotide pyrophosphorolysis, pH indicator-based assays were used to continuously follow dUTP hydrolysis (20, 21), but these methods are transparent to conformational changes of the enzyme. In this study, we took advantage of an intrinsic tryptophan sensor that we had recently engineered in the C-terminal arm of hDUT (Trp^{158}) (13) to resolve the fundamental steps of the enzymatic cycle using fast kinetic methods. Trp^{158} replaces a conserved phenylalanine residue that interacts with the uracil ring of dUTP (Fig. 1*C*) (12, 13). The mutational replacement of the benzene ring with an indole moiety did not perturb the enzyme activity (13). In the present study, the active site Trp^{158} sensor also allowed assessment of the proposed structural ordering of the C-terminal arm in the distinct enzyme-ligand complexes, relevant for the reaction cycle. Furthermore, we have developed a protocol for quenched-flow analysis, which is the first to allow the direct monitoring of the hydrolysis step of a dUTPase. We unambiguously show that the chemical step is rate-limiting and that the C-terminal arm is predominantly ordered in all enzymatic states.

EXPERIMENTAL PROCEDURES

Materials—The His-tagged nuclear isoform of human dUTPase (hDUT) and its F158W mutant construct ($hDUT^{W158}$) were expressed and purified as described previously (13, 22). Protein concentration was measured using the Bio-Rad protein assay reagent and by UV absorbance (λ_{280} = 10,430 M^{-1} cm^{-1} for hDUT and λ_{280} = 15,930 M^{-1} cm^{-1} for $hDUT^{W158}$) and is given in monomers. All measurements were carried out in 20 mM HEPES, pH 7.4, buffer, also containing 40 mM NaCl, 2 mM $MgCl_2$, and 1 mM dithiothreitol (unless otherwise stated), at 20 °C. dUMP, dUDP, dUTP, and α,β-imido-dUTP (dUPNPP) were purchased from Jena Bioscience (Germany), and [γ-^{32}P]ATP was from Izinta Ltd. Myosin was purified from rabbit skeletal muscle according to Ref. 23. Other reagents were from Sigma.

Enzyme Activity—Enzyme activity was measured in steady-state pH indicator-based assays as described in Ref. 20 and was typically found to be 6 ± 2 s^{-1}. Active site titration was used to determine K_M and also to evaluate the active fraction of hDUT and $hDUT^{W158}$ preparations. In the absorbance stopped-flow setup, an assay buffer containing 100 μM phenol red indicator and 1 mM HEPES, pH 7.5, provided optimal monitoring of dUTP hydrolysis. To avoid mixing artifacts, the enzyme was dialyzed in this assay buffer prior to active site titration. Measured time courses (*cf.* Fig. 3*C*) were subjected to global fit analysis using GEPASI (24). The floated parameters were k_1, k_{-1}, k_2, and [*E*] of the Michaelis-Menten scheme,

$$E + S \underset{k_{-1}}{\overset{k_1}{\rightleftharpoons}} ES \xrightarrow{k_2} EP$$

SCHEME 1

where $K_M = (k_{-1} + k_2)/k_1$ and $k_2 = k_{cat}$.

The inactive protein fraction in the measured hDUT or $hDUT^{W158}$ preparation was only in the range of the uncertainty of protein concentration determination (5–10%).

Fluorescence Spectra and Intensity Titrations—Fluorescence spectra and intensity titrations were recorded on a Jobin Yvon Spex Fluoromax-3 spectrofluorometer with excitation at 297 nm (slit 1 nm), emission between 320 and 400 nm (slit 5 nm), or at 347 nm. Because large concentrations of nucleotides were used, care was taken to correct for any additional fluorescence or inner filter effect imposed on the measured intensities by the nucleotide stock solutions.

Acrylamide Quenching—Acrylamide quenching was carried out by the addition of minute volumes of a 5 M acrylamide solution to the enzyme, enzyme-ligand, or *N*-acetyl-L-tryptophanamide (NATA) solutions. Raw data were corrected for the fluorescence arising from the acrylamide solution itself. F_0/F *versus* [Q] curves were analyzed using a modified Stern-Volmer equation (Equation 1),

$$F_0/F = 1 + K_{SV}[Q]\exp(V[Q]) \quad \text{(Eq. 1)}$$

where F_0 is the unquenched and F is the quenched fluorescence; Q is the quencher; K_{SV} is the dynamic (bimolecular) quenching constant; and V is the static (sphere of action) component of quenching (*cf.* Ref. 25).

Fluorescence Anisotropy—Fluorescence anisotropy was measured by the single-channel method in an Edinburgh Instruments FLS920P spectrofluorometer equipped with Glan-Thompson prism polarizers. Tryptophan emission spectra (λ_{ex} = 295 nm, λ_{em} = 320–400 nm) were recorded at four different polarizer configurations (VV, VH, HV, and HH, where V and H denote vertical and horizontal polarizer configurations, respectively, the first letter being designated to the excitation, the second to the emission polarizer). After base-line correction, anisotropy was calculated for the entire spectrum using Equation 2,

$$r = (I_{VV} - GI_{VH})/(I_{VV} + 2GI_{VH}) \quad \text{(Eq. 2)}$$

where r is anisotropy, I is fluorescence intensity, and $G = I_{HV}/I_{HH}$ is a wavelength-dependent parameter of the instrument setup.

Stopped-flow Experiments—Measurements were done using either an SF-2004 (KinTek Corp., Austin, TX) or a SFM-300 (Bio-Logic SAS) stopped-flow apparatus. Tryptophan fluorescence was excited at 297 nm, and emission was selected with a band-pass filter having a peak in transmittance at 340 nm. Time courses were analyzed using the curve fitting software provided with the stopped-flow apparatus or by Origin 7.5 (OriginLab Corp., Northampton, MA).

[γ-^{32}P]dUTP Synthesis—All synthesis reactions were carried out in a buffer containing 25 mM Tris, pH 7.4, and 100 mM NaCl. Autophosphorylation of 20 μM nucleoside diphosphate kinase (NDPK; from yeast; catalog number N0379; Sigma) was carried out in 5 mM EDTA at 30 °C for 10 min in a final volume of 100 μl using 20 μM [γ-^{32}P]ATP, according to Ref. 26. To remove ADP and [γ-^{32}P]ATP from the reaction in a quick manner, we applied batch adsorption on anion exchanger

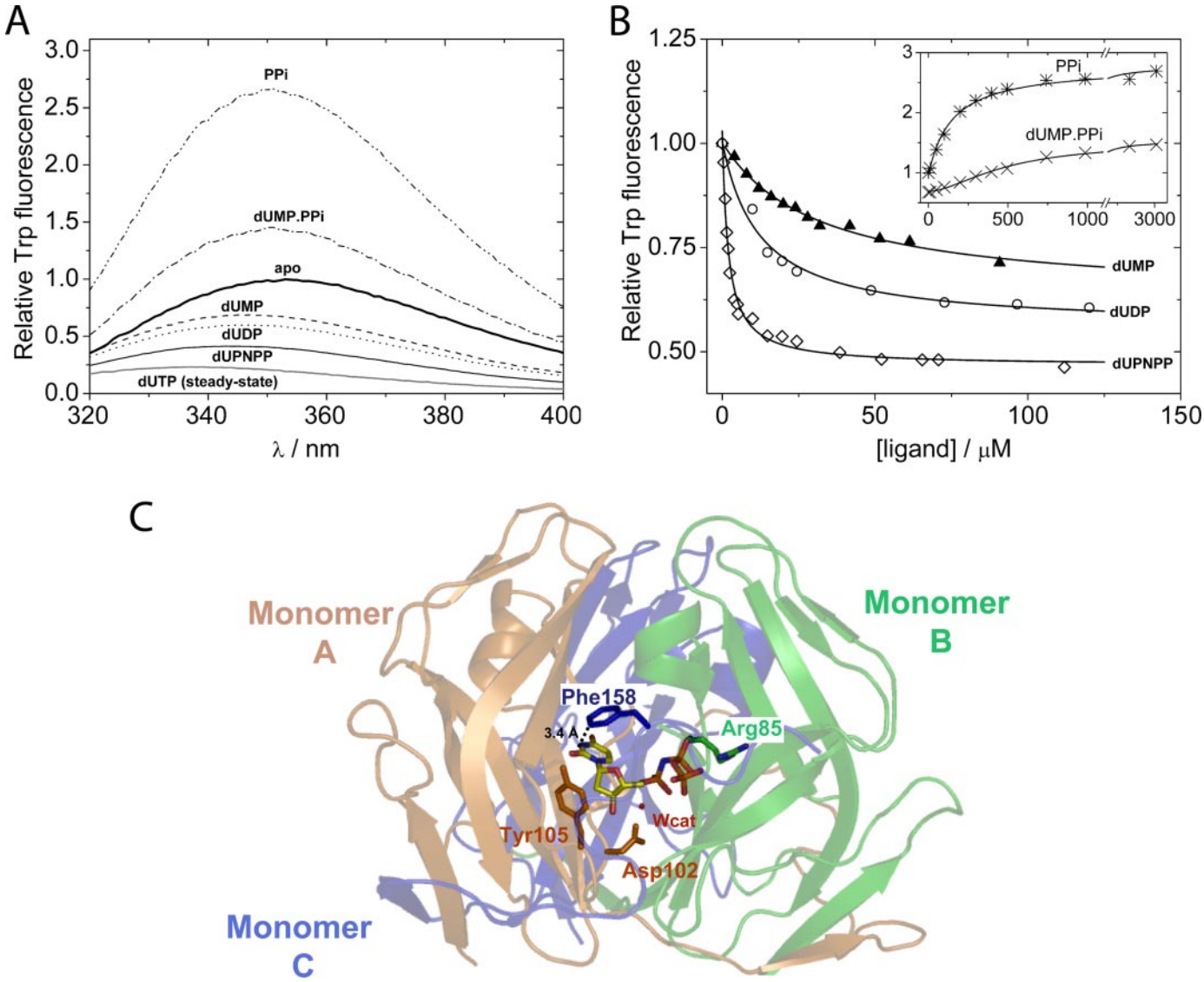

FIGURE 1. *A*, fluorescence emission spectra of hDUT^{W158} at saturating concentrations of ligands. λ_{ex} = 295 nm, data are normalized to the emission peak of the apo enzyme. [hDUTW158] = 4 μM, [dUMP] = 500 μM, [dUDP] = 300 μM, [dUPNPP] = 100 μM, [dUTP] = 2 mM, [PP_i] = 5 mM. To capture the dUTP-bound cycling steady state, a high excess of dUTP was used, and the spectrum was recorded within 30 s after dUTP was added. For analysis of fluorescence spectral parameters, see Table 1. *B*, fluorescence equilibrium titration of hDUT^{W158} with its ligands. λ_{ex} = 295 nm, λ_{em} = 347 nm; *solid lines* represent quadratic fits to the data except for the dUMP·PP_i curve, where a Hill equation with n = 1.7 provided a better fit. K_d values from the presented fits are as follows: 31 ± 4 μM for dUMP (*triangles*), 12 ± 2 μM for dUDP (*circles*), 1.9 ± 0.2 μM for dUPNPP (*diamonds*) (in the *inset*, 146 ± 15 μM for PP_i (*stars*) and 494 ± 25 μM for dUMP·PP_i (*crosses*)). The dUMP·PP_i titration was carried out by titrating dUMP-saturated enzyme (in 500 μM dUMP) with PP_i. *C*, three-dimensional structure of hDUT in complex with dUPNPP (figure produced using Protein Data Bank code 2HQU (13) and PyMOL). The three monomers (*A–C*) are represented by *color-coded schematic diagrams*. One of the three active sites is shown with the bound dUPNPP (*stick model*; *yellow* carbons and otherwise atomic *coloring*). The Phe^{158} residue (monomer C) stacks over the uracil ring. Other coordinating residues from monomers A and B and the catalytic water molecule (*red sphere*, labeled W_{cat}) are shown for orientation purposes.

resin in an expectation that the resin will only remove the negatively charged nucleotides and will not bind NDPK. The NDPK isoenzyme used in the experiment has a calculated pI of 8.65 and therefore carries a net positive charge at pH 7.4. According to the expectation, 25 μl of washed Q-Sepharose (Amersham Biosciences) added to the autophosphorylation reaction mixture immobilized all nucleotides without binding NDPK. The Q-Sepharose beads were then removed from the reaction by a 30-s centrifugation step. Subsequently, 25 μM dUDP and 10 mM Mg^{2+} were added to [^{32}P]NDPK to yield [γ-^{32}P]dUTP (incubation for 10 min at 30 °C). The enzyme was then completely removed from the [γ-^{32}P]dUTP-containing solution by phenol extraction that was carried out according to Ref. 27. For the analysis of the synthesis products (see "Results"), the radioactive nucleotide and phosphate contents were separated from each other using charcoal adsorption (as in Ref. 28). The advantage of using charcoal is that it binds all nucleotides but not P_i and PP_i. Radioactivity was counted in water in a Wallac 1409 liquid scintillation counter. We used a [γ-^{32}P]ATP stock solution of high specific activity (0.4 MBq/μl, 111 GBq/μmol) to obtain a similarly high specific activity [γ-^{32}P]dUTP sample suitable for tracing. The synthesized [γ-^{32}P]dUTP was added to a large molar excess of nonlabeled bulk dUTP in a 1:100 volume ratio. For further details of the analysis of the synthesis products, see "Results."

TABLE 1

Fluorescence properties of hDUT^{W158} apoenzyme and its ligand-bound complexes

For comparison, the respective fluorescence characteristics of NATA, representing free tryptophan, are also given. NA, not applicable.

Ligand	K_d	λ_{max}	Relative fluorescence	K_{SV}	V	Anisotropy
	μM	nm		m^{-1}		
None		353	1	6.6 ± 0.12	0.9 ± 0.06	0.077 ± 0.005
dUMP	32 ± 2	347	0.64 ± 0.03	6.1 ± 0.13	0.4 ± 0.07	0.081 ± 0.003
dUDP	12 ± 1	347	0.59 ± 0.03	5.7 ± 0.10	0.6 ± 0.05	0.085 ± 0.006
DUTP	<1	339	0.20 ± 0.06			
dUPNPP	5 ± 3	343	0.40 ± 0.04	5.0 ± 0.09	0.4 ± 0.05	0.091 ± 0.003
dUMP.PPi	479 ± 20	351	1.40 ± 0.01	6.0 ± 0.2	0.9 ± 0.10	0.106 ± 0.002
Ppi	146 ± 15	351	2.53 ± 0.02	6.8 ± 0.19	1.5 ± 0.08	0.112 ± 0.002
NATA (in the absence of protein)	NA	355	NA	17.4 ± 0.12	1.9 ± 0.02	0.0044 ± 0.0008

Quenched-flow Experiments—Quenched-flow experiments were carried out using the RQF-3 (KinTek Corp., Austin, TX) quenched-flow apparatus. 2 M HCl (⅔ M in the reaction) was used as the chemical quencher of the dUTPase reaction. Hydrolysis products were separated according to Ref. 28. The amount of the resulting $^{32}PP_i$ product was counted in water using a Wallac 1409 liquid scintillation counter (PerkinElmer Life Sciences).

Data Analysis and Numerical Simulations—Data analysis and numerical simulations were done using Origin 7.5 (OriginLab Corp., Northampton, MA) or the freely available GEPASI 3 biochemical kinetics simulation software (24), respectively.

RESULTS

Fluorescence Spectral Properties of hDUT^{W158} and Its Ligand-bound Complexes—Recently, fluorescence emission from the Trp^{158} fluorophore was shown to be significantly and characteristically quenched in dUTPase-dUPNPP and dUTPase-dUMP complexes as compared with the apoenzyme (13), in agreement with the expectation that the stacking between conserved residue Phe^{158} and the substrate uracil ring (*cf.* Fig. 1*C*) is also present in the Trp^{158} mutant enzyme. Following these observations, we quantified maximal fluorescence changes and spectral shifts of Trp^{158} upon binding to physiological ligands and to the nonhydrolyzable substrate analogue dUPNPP (Fig. 1*A* and Table 1). These data yield information on the interaction of Trp^{158} with the uracil moiety of any bound nucleotide and will allow interpreting the fluorescence-based kinetic experiments. The Trp^{158} fluorescence emission maximum of the apoenzyme was at 353 nm, a typical value for a nonburied protein tryptophan ($\lambda_{max,\ NATA}$ = 355 nm) (25) (Fig. 1*A*). Fig. 1*A* also shows that the binding of different uracil nucleotides but not that of PP_i to hDUT^{W158} quenches Trp^{158} fluorescence, probably due to aromatic stacking between the indole and uracil rings (shortest distances between atoms of the uracil moiety and those of the Phe^{158} benzene ring in hDUT are 3.4–3.7 Å, as determined in the crystal structure of the enzyme-dUPNPP complex, Protein Data Bank code 2HQU) (13) (Fig. 1*C*). The magnitude of the nucleotide-induced quench and blue shift increased in the order dUMP → dUDP → dUPNPP (Table 1). This implies that the presence of the β- and γ-phosphates causes the C-terminal arm to form more interactions with the phosphate chain of the substrate (in agreement with the structural description (13)), whereby the arm may become less flexible and may stabilize the stacking interaction between Trp^{158} and the uracil ring. Interestingly, Trp^{158} fluorescence was even more quenched during steady-state dUTPase cycling than in any of the other ligand-bound states (Fig. 1*A*). This suggests that there is at least one major steady-state intermediate that cannot be produced by the addition of the above ligands (*e.g.* the prehydrolysis mimic dUPNPP or the posthydrolysis mimic dUMP·PP_i states). A possible explanation for this finding is that a particular protein conformational change occurs in the presence of dUTP (but not in the presence of dUPNPP or other nucleotides), leading to the hydrolysis-competent state (see below).

The large fluorescence increase in the presence of PP_i indicates that the binding of this ligand also causes a conformational change in the active site. Control experiments conducted with bovine serum albumin and NATA (data not shown) ascertained that the effect of PP_i on our tryptophan sensor was specific. Interestingly, a rather similar phenomenon was observed in an earlier study in which a tryptophan engineered into the entrance of the nucleotide binding site of myosin (Trp^{129}, in close proximity to the adenine moiety of ATP) exhibited a large quench on nucleotide binding and a large fluorescence increase on PP_i binding (29). We probed the potential interaction of hDUT^{W158} with phosphate (P_i) (used at high excess), but no signal change was detected.

Fluorescence Intensity Titrations to Determine Enzyme-Ligand Dissociation Constants—Fig. 1*B* shows fluorescence intensity titrations of 4 μM hDUT^{W158} with various ligands (enzyme active site concentrations are used throughout this paper). Dissociation constants are given in Table 1. K_d values illustrate that the affinity of hDUT^{W158} increases in the order dUMP → dUDP → dUPNPP, with dUDP and dUPNPP binding being 3 and 10 times stronger than that of dUMP, respectively. dUTP binding cannot be measured using this equilibrium method, but we anticipate that its K_d value may be equal to or lower than that of dUPNPP ($K_d \sim 1$ μM). Nucleotide-free hDUT^{W158} exhibited a K_d for PP_i of 146 μM. The dissociation constant of PP_i for the ternary enzyme products complex (E·dUMP·PP_i) was about 3 times larger than that for E·PP_i. This moderate antagonistic effect between the binding of dUMP and PP_i to the enzyme is probably due to the repulsion between the negative charges of dUMP and PP_i.

Acrylamide Quenching—We have performed acrylamide quenching experiments with hDUT^{W158} to monitor the solvent accessibility of the Trp^{158} reporter (Fig. 2*A*, Table 1). For reference and control, we also measured properties of NATA, a model compound for a rotationally free and maximally solvent-

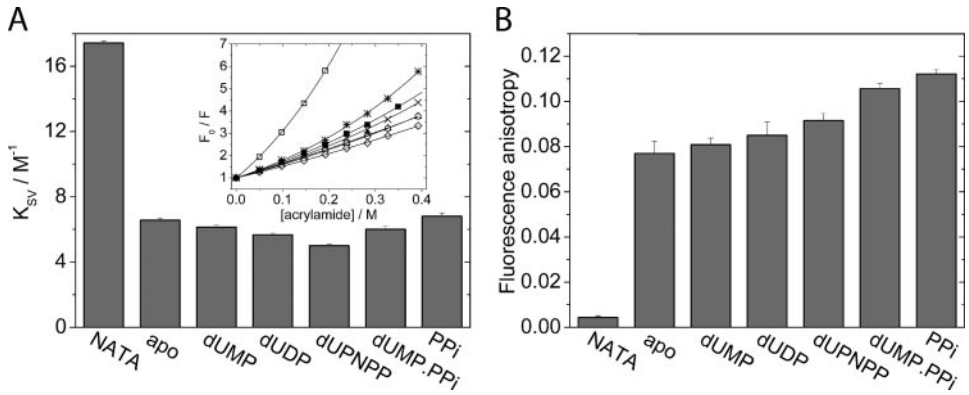

FIGURE 2. **Solvent accessibility and anisotropy of hDUT^{W158} complexed with various ligands.** *A*, 4 μM hDUT^{W158} with or without saturating concentrations of specific ligands was titrated using a 5 M acrylamide stock solution (*inset*). *Lines* on the data points are fits to the modified Stern-Volmer equation (Equation 1). The dynamic quenching components (K_{SV} values) of the fits are shown as *bars*. 1 μM NATA was used to represent a fully accessible tryptophan. *Error bars*, fitting errors. *B*, steady-state anisotropy of Trp^{158}. Concentrations are the same as in Fig. 1*A*. *Error bars*, S.D. of the data points obtained for each emission wavelength. 1 μM NATA was used to represent a tryptophan exhibiting maximal rotational diffusion.

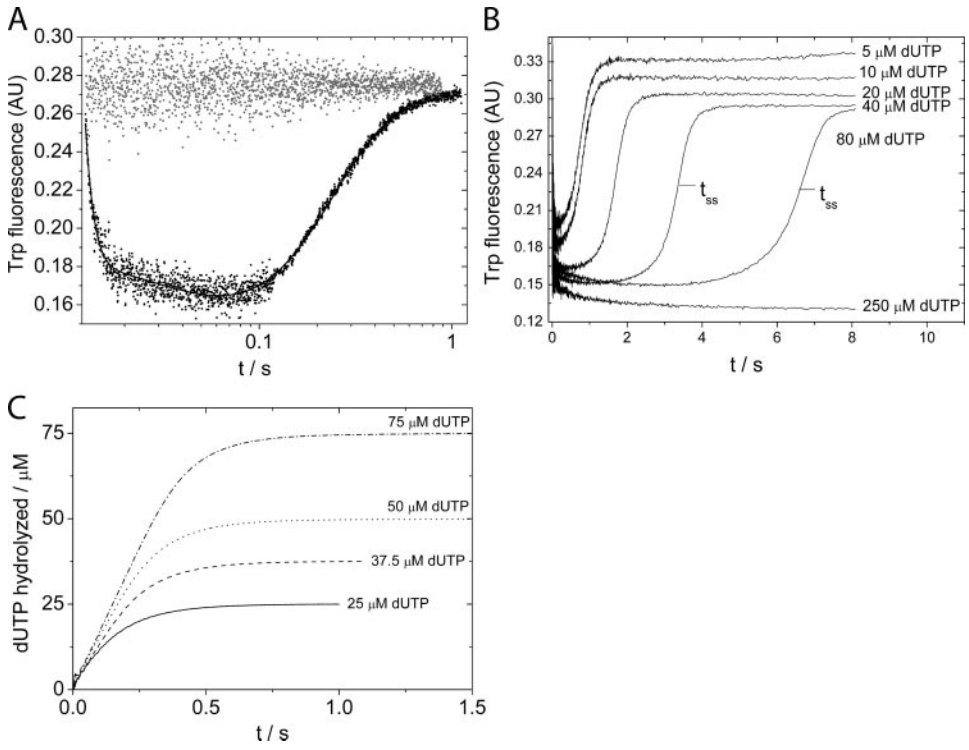

FIGURE 3. **hDUT^{W158} single turnovers as monitored using intrinsic (*A* and *B*) and extrinsic (*C*) signals.** *A*, tryptophan fluorescence stopped-flow traces of 7.5 μM hDUT^{W158} mixed with 5.25 μM dUTP (*black points*) or with buffer (*gray points*). Fluorescence was recorded at λ_{ex} = 295 nm and λ_{em} = 340 nm. *Solid line*, a triple exponential fit to the data with parameters $A_1 = 0.097$, $k_1 = 912\ s^{-1}$ for dUTP binding, $A_2 = 0.193$, $k_2 = 14\ s^{-1}$ for a first order isomerization, $A_1 = -0.269$, $k_2 = 6.7\ s^{-1}$ for the chemical step. *B*, tryptophan fluorescence stopped-flow traces of 5 μM hDUT^{W158} mixed with various concentrations of dUTP. *C*, 58 μM hDUT^{W158} mixed with 25, 37.5, 50, or 75 μM dUTP in the stopped-flow in the presence of 100 μM phenol red indicator. Absorbance was recorded at λ = 559 nm to monitor the release of protons upon dUTP hydrolysis. Curves at substoichiometric dUTP concentrations appear as single exponentials, whereas at higher dUTP concentrations, a linear steady-state phase can be observed. Global fits to all curves using the k_1, k_{-1}, and k_2 floating parameters of the Michaelis-Menten scheme (Scheme 1) yielded $K_M = 3.6 \pm 1.9\ \mu M$, $k_{cat} = 6.7 \pm 0.2\ s^{-1}$.

accessible tryptophan residue. Acrylamide titrations of the Trp^{158} fluorescence intensity are displayed as Stern-Volmer plots (Fig. 2*A*, *inset*) with a modified Stern-Volmer equation (Equation 1) fitted to the data points to separate the dynamic component (described by the K_{SV} quenching constant) from the static quenching sphere of action (V) (25). Compared with our measurement on NATA and literature data on K_{SV} values for tryptophans in short peptides (10–14 M^{-1}), Trp^{158} exhibits markedly reduced solvent accessibility (K_{SV} = 6.6 M^{-1}) even in the apoenzyme. Such a low K_{SV} was unexpected, considering that Trp^{158} is situated in the C-terminal arm of hDUT^{W158}, six residues away from the terminal amino acid. On the other hand, differences between K_{SV} values of various ligand-bound states of hDUT^{W158} are relatively small but significant (K_{SV}, ranging from 5.0 to 6.8 M^{-1}) (Fig. 2*A* and Table 1). This finding suggests that large conformational changes of the C-terminal arm upon ligand binding are unlikely to occur. The solvent accessibility of Trp^{158} decreases in the order dUMP → dUDP → dUPNPP, suggesting a gradual movement of the C-terminal arm toward the nucleotide. This observation is in line with our experiments shown in Fig. 1. Importantly, the solvent accessibilities of the *E*·dUMP·PP$_i$ and *E*·dUMP states were very similar, indicating that dUMP but not PP$_i$ induces shielding of the active site. PP$_i$ binding alone does not perturb the solvent accessibility of Trp^{158}, probably due to a relatively open active site conformation (Fig. 1).

Fluorescence Anisotropy—Fluorescence anisotropy is routinely used to describe the dynamic properties of a protein environment. Freely rotating small fluorophores are depolarized at room temperature and therefore exhibit anisotropies close to zero (*cf.* NATA in Fig. 2*B* and Table 1). We measured the steady-state anisotropies of apo-hDUT^{W158} and its ligand-bound complexes to gain further insights into the dynamic behavior of the C-terminal arm in various enzymatic states. The steady-state anisotropy of apo-hDUT^{W158} (r = 0.077) increased upon ligand binding, which reflects a steric hindrance of the fluorophore. Similarly to the previously described experiments (Figs. 1 and 2*A*), a correlation of the measured effect to the length of the phosphate chain of the nucleotide was observed (*i.e.* the value of r increased in the order apo → dUMP → dUDP → dUPNPP) (Fig. 2*B*). The largest increase in anisotropy was detected in the PP$_i$-

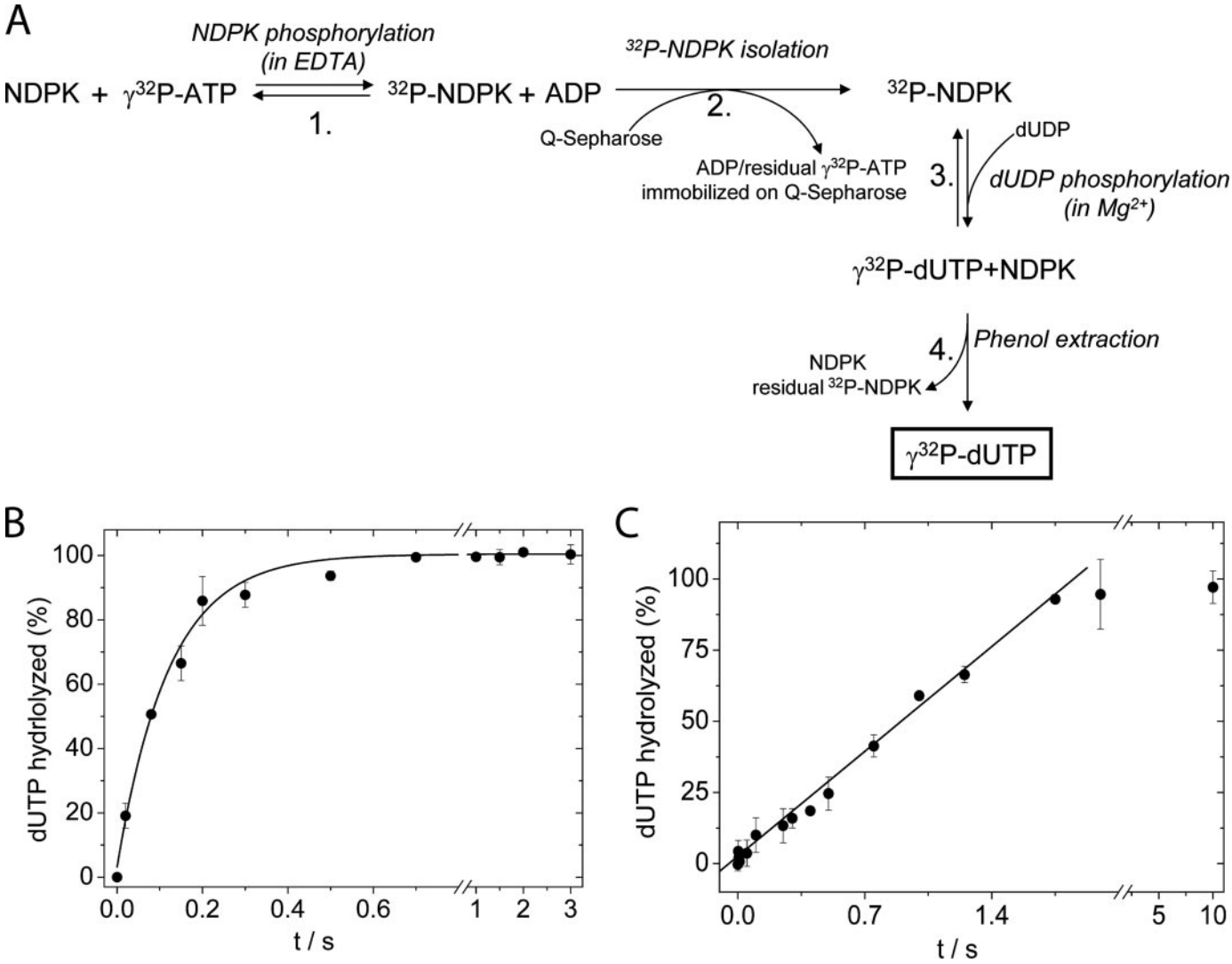

FIGURE 4. **[γ^{32}P]dUTP synthesis and quenched-flow measurements of dUTP hydrolysis.** *A*, scheme of [γ-^{32}P]dUTP synthesis. *Reactions 1* and *3* are highly reversible, while separation *steps 2* and *4* are very efficient, resulting in a [γ-^{32}P]dUTP compound that is free of contaminating radioactive nucleotides. Besides [γ-^{32}P]dUTP, the final product contains dUDP (<12.5 μM in our experiment) and $^{32}P_i$. If used as a tracer (>1:100 ratio), this preparation does not compromise the chemical purity of the bulk nucleotide solution. *B*, 100 μM hDUT and 50 μM [γ-^{32}P]dUTP were mixed (single turnover conditions), and the reaction was stopped with 1 M HCl after various incubation times. Hydrolysis was followed by measuring the relative amount of one of the hydrolysis products, the radioactive PP_i. Single exponential fits to the data (*solid line*) with $k_{obs} = 8.2 \pm 0.4\ s^{-1}$. *Error bars*, S.D. of three parallel measurements. *C*, the reaction of 18 μM hDUT^{W158} with 100 μM [γ-^{32}P]dUTP (5.6-fold excess) was followed in time. Linear fit to the data yielded a $k_{obs} = 2.9 \pm 0.04\ s^{-1}$ for the steady state. Lag or burst was not observed at the applied time resolution. *Error bars*, S.D. of three parallel measurements.

bound species ($E{\cdot}PP_i$ and $E{\cdot}dUMP{\cdot}PP_i$), although we previously showed that these are the most "open" and solvent-accessible enzyme states (Fig. 2*A*). Taken together, the anisotropy data indicate that (i) ligand binding to the polyphosphate binding site causes structural ordering of the C-terminal arm, proportionally to the length of the polyphosphate chain (without shielding Trp^{158} from the solvent); (ii) the lower anisotropy of uracil nucleotide-bound states compared with that of the $E{\cdot}PP_i$ state show that aromatic stacking to uracil slightly depolarizes Trp^{158} (Fig. 2*B* and Table 1).

Rapid Kinetics of hDUT^{W158} Followed by Intrinsic (Trp^{158}) and Extrinsic (Proton Release) Signals—In the knowledge of the fluorescence characteristics of individual enzyme-substrate (substrate analogue) and enzyme-product complexes (Fig. 1), progress curves obtained by monitoring Trp^{158} fluorescence during the interaction of hDUT^{W158} with dUTP in the stopped-flow yielded significantly more information than pH detection-based (proton release) methods. Fig. 3 shows single and multiple dUTP turnovers obtained using Trp^{158} fluorescence (*A* and *B*) or proton release (*C*) signals. Trp^{158} fluorescence traces of single dUTP turnovers ([*E*] > [S]) consisted of three exponential phases (Fig. 3*A*). A fast initial quench in fluorescence ($k_{obs} \sim 900\ s^{-1}$) was followed by an additional slower decrease ($k_{obs} \sim 20\ s^{-1}$), and then the fluorescence intensity returned to a close-to-initial value with a k_{obs} of $6.8 \pm 2.0\ s^{-1}$. In light of the steady-state fluorescence data of Fig. 1*A*, we interpret the first fast phase as the initial binding of the nucleotide in which Trp^{158} quenching occurs by stacking over the uracil ring. Considering the difference between the fluorescence intensity of the enzyme-dUPNPP complex and that during steady-state dUTPase cycling, the second slower phase can be interpreted as a dUTP-induced structural change that precedes or is concomi-

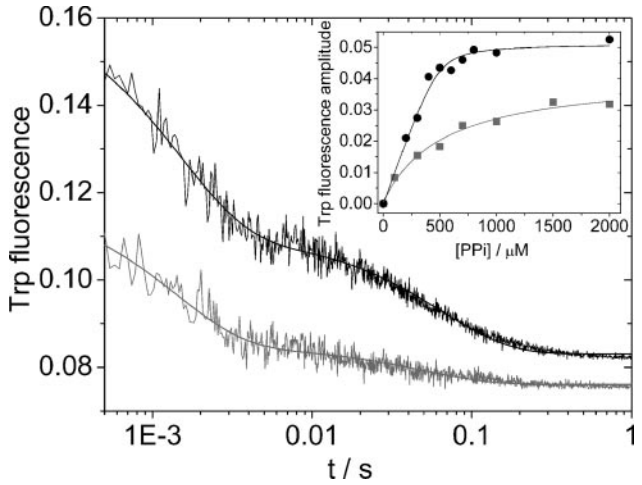

FIGURE 5. **Dissociation of PP_i measured by dUTP chasing in the stopped-flow.** Solutions of (4 μM $hDUT^{W158}$ + 2 mM PP_i) (*black trace*) or (4 μM $hDUT^{W158}$ + 300 μM dUMP + 2 mM PP_i) (*gray trace*) were mixed with 0.1 or 1 mM dUTP, respectively, in the stopped-flow. The observed fluorescence intensity change reports both the dissociation of products and the interaction with dUTP. Two exponentials fit to the data, with $A_1 = 0.053$ and $k_1 = 648\ s^{-1}$ for the fast phase and $A_2 = 0.027$ and $k_2 = 14\ s^{-1}$ for the slow phase (*black trace*) or with $A_1 = 0.032$ and $k_1 = 705\ s^{-1}$ for the fast phase and $A_2 = 0.0087$ and $k_2 = 20\ s^{-1}$ for the slow phase (*gray trace*) ($k_{obs} = 726 \pm 46, 15 \pm 0.9\ PP_i$, $684 \pm 84, 18 \pm 2.5$ dUMP·PP_i). *Inset*, PP_i concentration dependence of the fast phase amplitude (A_1). 4 μM $hDUT^{W158}$ was mixed with different concentrations of PP_i either in the absence (*black circles*) or in the presence (*gray squares*) of 300 μM dUMP. dUTP chase was accomplished by mixing with 0.1 or 1 mM dUTP (*black circles* or *gray squares*, respectively). Quadratic fits to the A_1 data of the recorded fluorescence time courses yielded an apparent K_d of 327 ± 117 μM for PP_i (*black circles*) and 532 ± 128 μM for PP_i binding to E·dUMP (*gray squares*).

tant with dUTP hydrolysis. The third phase reflects the slowest rate-limiting step of the cycle (dUTP hydrolysis or product release). (The identities of the steps associated with the second and third phases were clarified in subsequent experiments (Figs. 4 and 5).) Determination of the substrate concentration dependence of the rate constant of the first phase under pseudo-first order conditions was challenging, because either the signal/noise ratio was too low for reasonable resolution (when attempting to decrease [S] at a constant [*E*] (maintaining [S] ≪ [*E*])), or the amplitude became completely lost in the dead time of the stopped-flow apparatus (when applying a severalfold excess of [S] over the lowest detectable [*E*]). Measurements carried out using near-equimolar concentrations of enzyme and substrate indicated that the time course of this phase does depend on concentration (k_{obs} values of force-fitted exponentials were 400–1200 s^{-1} in the applied 2.5–15 μM concentration range). Numerical simulations in which this phase was assigned to a second-order binding step showed good agreement with the experimental traces, and the fundamental rate constants could be extracted (*cf.* Fig. 6*A* and Table 2). We did not observe systematic concentration dependence of the k_{obs} (termed $k_{ISO,obs}$ in Table 2) of the second exponential phase (20 ± 18 s^{-1}), which confirms the first order nature of this proposed isomerization step (Fig. 3*B*). The k_{obs} value of the third phase did not exhibit concentration dependence in the single turnover concentration regime. The k_{obs} of this phase was in good agreement with the previously determined steady-state k_{cat} of hDUT (8 ± 3 s^{-1}) (13), indicating that it represents the rate-limiting step of the dUTPase cycle. Furthermore, the duration of the steady state (t_{ss}) in multiple turnover Trp^{158} fluorescence traces (*i.e.* the time elapsed between the start of the reaction and the inflection point of the fluorescence restoration phase) (Fig. 3*B*) was consistent with the above third phase k_{obs} and steady-state k_{cat} values ($t_{ss} \approx [S]_{initial}/([E]_{total}k_{cat})$, if $[S]_{initial} \gg K_M$).

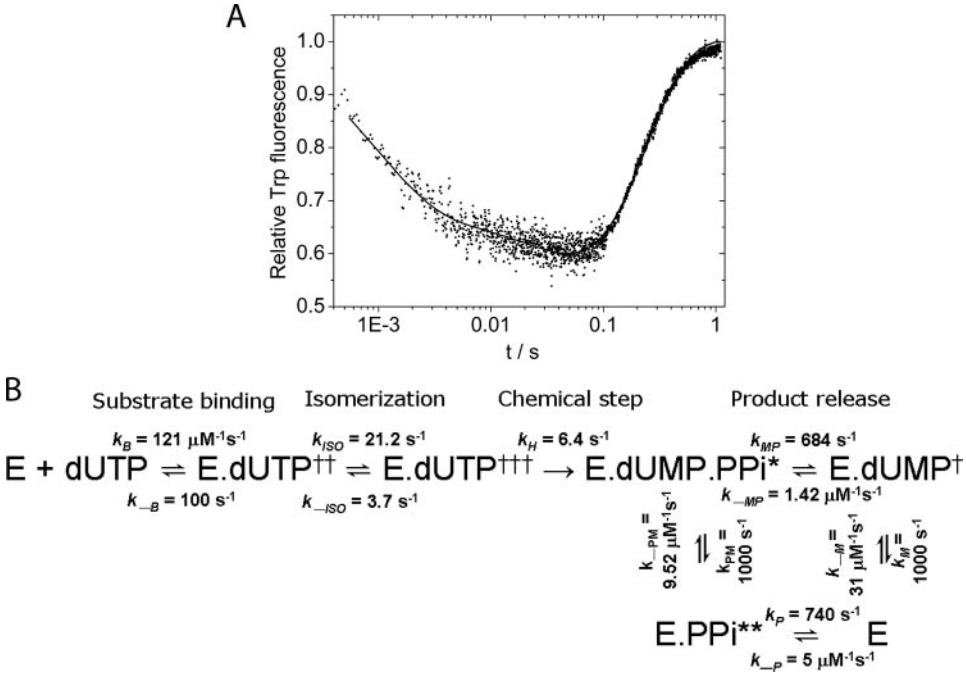

FIGURE 6. **Kinetic modeling of the human dUTPase enzymatic cycle.** *A*, taking the same example as in Fig. 3*A*, a time course upon mixing 7.5 μM $hDUT^{W158}$ with 5.25 μM dUTP is shown, prepared for global fitting (fluorescence normalized to the apoenzyme, dead time considered). The *solid line* is a global fit to the data points using the kinetic model shown in *B* and the relative fluorescence changes in Table 1. *B*, kinetic model of the hDUT enzymatic cycle. *Daggers* and *stars* indicate fluorescence decrease or increase compared with the apoenzyme, respectively. The rate constants shown in the model were used as parameters of the kinetic simulation (*A*) and are compiled in Table 2. For the k_{-PM}/k_{PM} and k_{-M}/k_M rate constant pairs, only the ratios (defined by K_d values of Tables 1 and 2) and the lower bounds for the rate constant pairs are known. These lower bounds were used in the numerical simulations as shown. Increases in the values of these rate constants (while keeping their respective ratios constant) did not cause any detectable change in the enzyme mechanism.

Fig. 3*C* shows single and multiple turnovers detected by a proton release assay in an absorbance stopped-flow setup. The amplitude of the curves was directly proportional to the initial substrate (and thus the released proton) concentration. In single turnover conditions ([*E*] > [S], lower two curves in Fig. 3*C*), the time courses corresponded to single exponentials, and k_{obs} values (6.5 ± 0.1 s^{-1}) were identical to the steady-state k_{cat} of the enzyme (Table 2). In multiple turnovers (*upper two curves* in Fig. 3*C*) a linear steady-state phase was observed without any burst of proton release. These profiles altogether imply that the enzymatic cycle is limited by a single rate-limiting step that occurs before

TABLE 2
Kinetic parameters of the hDUT enzymatic cycle

	Value	Source experiment	Figure
k_{cat} (s^{-1})	8 ± 3	Steady-state proton release assay (13)	
	6.8 ± 2.0	Fluorescence single turnovers	3, *A* and *B*
	6.5 ± 0.1	Proton release turnovers	3*C*
	6.7 ± 0.2		3*C*
K_M (μM)	3.6 ± 1.9	Michaelis-Menten global fits to proton release turnovers	3*C*
k_{cat}/K_M (M^{-1} s^{-1})	1.9×10^6		3*C*
k_B (s^{-1})	120	Global fit to fluorescence traces	6, *A* and *B*
k_{-B} (μM^{-1} s^{-1})	100		6, *A* and *B*
$k_{ISO, obs}$ (s^{-1})	20 ± 18	Fluorescence turnovers[a]	3, *A* and *B*
	24 ± 6	dUTP chasing[a]	5
k_{ISO} (s^{-1})	21.2	Global fit to fluorescence traces	6, *A* and *B*
k_{-ISO} (s^{-1})	3.7		
k_H (s^{-1})	5.5 ± 2.5	Quenched-flow single turnover	4*A*
	6.4	Global fit to fluorescence traces	6, *A* and *B*
k_{MP} (s^{-1})	684 ± 84	Fluorescence PP_i chasing from *E*·dUMP·PP_i	5
k_{-MP} (μM^{-1} s^{-1})	1.42	k_{MP}/K_d(*E*·PP_i for dUMP)[b]	5 and 6, *A* and *B*
k_{PM} (s^{-1})	>1000	Fluorescence stopped-flow[c]	6, *A* and *B*
k_{-PM} (μM^{-1} s^{-1})	> 9.5	k_{PM}/K_d (*E*·PP_i for dUMP)[d]	6, *A* and *B*
k_M (s^{-1})	>1000	Fluorescence stopped-flow[c]	6, *A* and *B*
k_{-M} (μM^{-1} s^{-1}	>31	k_M/K_d (*E* for dUMP)[b]	6, *A* and *B*
k_P (s^{-1})	740 ± 66	Fluorescence PP_i chasing from *E*·PPi	5
k_{-P} (μM^{-1} s^{-1})	5	k_P/K_d (*E* for PP_i)[b]	5 and 6, *A* and *B*

[a] $k_{ISO, obs} = k_{ISO} + k_{-ISO}$.
[b] K_d values for different ligands are listed in Table 1.
[c] The reaction was practically completed in the dead time of the stopped-flow (<1 ms).
[d] K_d (*E*·PP_i for dUMP) calculated as K_d (*E* for dUMP)K_d(*E*·dUMP for PP_i)/K_d (*E* for PP_i).

or is concomitant with proton release. We could model these proton release events with Michaelis-Menten kinetics in which a rapid equilibrium (k_1, k_{-1}) precedes the rate-limiting step ($k_2 = k_{cat}$). Global fits to the single and multiple turnover time courses using the k_1, k_{-1}, and k_2 floating parameters of Scheme 1 yielded $K_M = 3.6 \pm 1.9$ μM, $k_{cat} = 6.7 \pm 0.2$ s^{-1}, $k_{cat}/K_M \sim 1.9 \times 10^6$ M^{-1} s^{-1}, for both hDUT and hDUT^{W158} proteins.

[γ-^{32}P]dUTP Synthesis—[γ-^{32}P]dUTP is not commercially available. We therefore developed a straightforward synthesis method (Fig. 4*A*) using NDPK that converts [γ-^{32}P]ATP and dUDP into [γ-^{32}P]dUTP and ADP by a ping-pong mechanism (26, 30). We took advantage of the fact that the phosphorylated enzyme intermediate of the NDPK reaction is long lived in the absence of Mg^{2+} and thus can be separated from the phosphate donor nucleotides (26). The resulting synthesis product (after step 4 in Fig. 4*A*) contains [γ-^{32}P]dUTP, dUDP, and inorganic phosphate. To test for the presence of any non-dUTP-derived radiolabeled species that would compromise radiochemical purity, aliquots of the synthesis product were fully hydrolyzed by (i) dUTPase (extremely specific for dUTP), (ii) dUTPase + myosin (hydrolyzes NTPs (31)), or (iii) apyrase (hydrolyzes (d)NTPs and (d)NDPs (32)). All three enzyme conditions resulted in liberation of the same $^{32}P_i$ content of the total radioactive material, demonstrating that practically all hydrolyzable radioactive nucleotide species in the synthesis product was [γ-^{32}P]dUTP. The synthesis product contained 15 ± 3% non-nucleotide $^{32}P_i$ (measured in samples from which all nucleotides had been removed). Analysis showed that this fraction originated from (i) carryover from the original [γ-^{32}P]ATP solution (5%), (ii) spontaneous hydrolysis of γ-^{32}P-labeled nucleotides during the four-step procedure, and possibly (iii) slow $^{32}P_i$ release from the phosphorylated NDPK in the absence of phosphate acceptor (during step 2). The ~15% $^{32}P_i$ in the synthesis product does not reflect the P_i content of the bulk solution to be used in quenched-flow experiments, because a subsequent large dilution of the synthesis product in nonlabeled dUTP decreased the P_i/dUTP concentration ratio to less than 1:10,000 in the reagent solution used in the quenched-flow assay. The only noticeable effect of the condition that ~15% of the total radioactivity was radioactive $^{32}P_i$ was the reduction of the maximal expected signal change from 100 to 85%, which did not impede the evaluation of quenched-flow results. Similarly, the dUDP concentration of the synthesis product was drastically reduced by the dilution of [γ-^{32}P]dUTP in a large molar excess of nonlabeled dUTP (the dUDP/dUTP molar ratio was less than 1:1600 in the assay reagent). In the above described experimental conditions, the most important factor in providing chemical purity was the use of high quality nonlabeled nucleotide to be traced with a high specific activity radioactively labeled one. The total [γ-^{32}P]dUTP yield was calculated following the analysis of the radioactive constitution of the synthesis product and was found to be 25% (*i.e.* one-quarter of the [γ-^{32}P]ATP was converted specifically into [γ-^{32}P]dUTP). Considering that both reactions 1 and 3 (Fig. 4*A*) are fully reversible, this yield indicates that the procedure was highly efficient.

Direct Observation of the Chemical Step by Quenched-flow Using [γ-^{32}P]dUTP—Fig. 4*B* shows a single turnover experiment with a single exponential fit to the data points. For both wild-type hDUT and hDUT^{W158} constructs and depending on the protein preparation, the k_H of single turnovers was determined to be 5.5 ± 2.5 s^{-1}, in agreement with the k_{obs} values observed in the fluorescent and proton release turnovers (Table 2). There was no systematic difference between the k_H values of hDUT and hDUT^{W158}. When excess dUTP was mixed with hDUT (Fig. 4*C*), we observed a linear steady-state phase without any burst, clearly arguing that the rate-limiting step of the dUTPase enzymatic cycle is identical to (or precedes) the chemical step.

Product Release—The large fluorescence intensity change of Trp^{158} induced by PP_i binding allowed us to follow the dissociation of PP_i from the enzyme. We carried out dUTP chase

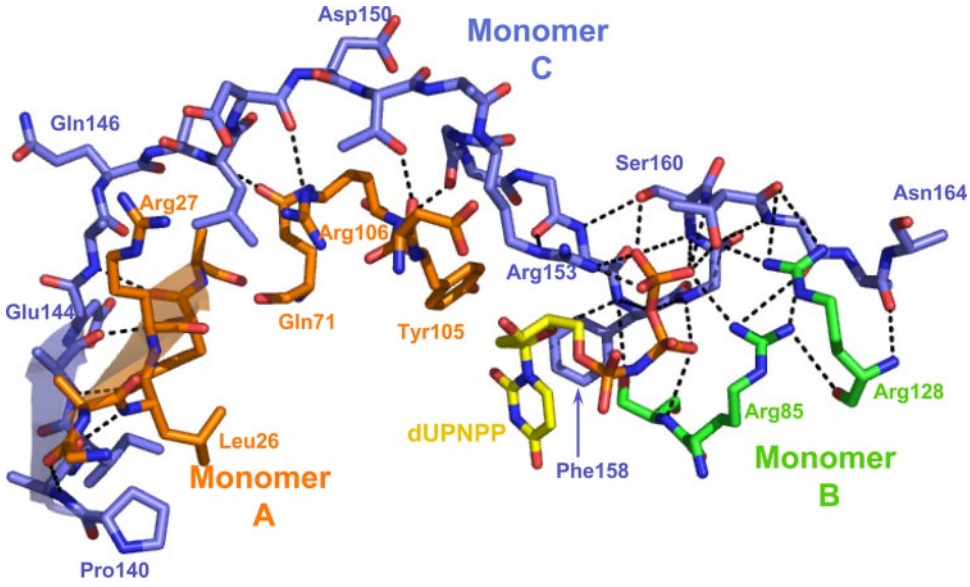

FIGURE 7. **Interactions of the C-terminal arm of hDUT with adjacent monomers and dUPNPP.** The *arrows* in the *lower left part* of the model depict β strand interactions between residues 140–144 of the C-terminal arm of monomer C (atomic *coloring* with *blue* carbons) and the N terminus of monomer A (atomic *coloring* with *orange* carbons). Residues 149–155 of monomer C are involved in contacts with side chain and main chain atoms within the conserved motif 3 of monomer A that accommodates the deoxyribose and the uracil rings of the substrate. Arm residues 155–160 contact mostly ligand atoms (*stick model*, atomic *coloring* with *yellow* carbons) and each other. The last C-terminal residues (residues 160–163) engage in extensive hydrogen bonding to the atoms of monomer B (*stick model*, atomic *coloring* with *green* carbons). Structural data are taken from Ref. 13 (Protein Data Bank code 2HQU).

experiments to avoid rebinding of the dissociated PP_i. Upon mixing the E·PP_i complex with excess dUTP in the stopped-flow, double exponential curves were recorded (Fig. 5, *upper black trace*) having a fast phase of 740 ± 66 s^{-1} and a slow phase of 24 ± 6 s^{-1}. The amplitude of the fast but not the second slow phase depended upon the concentration of PP_i (Fig. 5, *inset*). The first phase can therefore be attributed to PP_i dissociation, whereas the second phase arises from the isomerization of the ES complex occurring after the initial dUTP binding step (*cf.* Fig. 3*A*). The K_d value resulting from a one-binding site quadratic fit to the amplitude data (327 ± 117 μM) was similar to that obtained from equilibrium titrations (*cf.* Fig. 1*B* and Table 1). Product dissociation was measured also from the *E*·dUMP·PP_i complex (Fig. 5, *gray trace*). Curves exhibited k_{obs} values (684 ± 84 s^{-1}) similar to those of the *E*·PP_i curves, showing that the rate constants of PP_i dissociation from *E*·PP_i and *E*·dUMP·PP_i are similar (Table 2). In line with the lower initial fluorescence level of *E*·dUMP·PP_i compared with that of *E*·PP_i (*cf.* Fig. 1*A*), the amplitudes of the *E*·dUMP·PP_i chasing traces were lower than those of the *E*·PP_i chasing traces (Fig. 5). Binding and dissociation of dUMP was too fast to observe by stopped-flow.

Kinetic Modeling of the hDUT Enzymatic Cycle—The measured accessible parameters of the hDUT enzymatic cycle (Tables 1 and 2) allowed us to propose a model that provided good fits to our experimental data (Fig. 6*B*). Using this model, kinetic simulations of the $hDUT^{W158}$ fluorescence profile during dUTP hydrolysis yielded time courses that were very similar to the measured ones (Fig. 6*A*). Parameters for the binding (k_B, k_{-B}), isomerization (k_{ISO}, k_{-ISO}) and hydrolysis (k_H) steps were floating parameters, given that these are the events that primarily determine the fluorescence profiles during dUTP turnovers. Kinetic parameters of the product release steps were fixed so that the ratios of the dissociation and association rate constants of the individual steps yield the K_d values shown in Table 1 and thus determine the final fluorescence levels. The rate constants of product release are so fast compared with the rate-limiting step that they do not influence the turnover curves.

DISCUSSION

A central aspect of the present study is that the fluorescent signal of a single tryptophan engineered into the C-terminal arm of hDUT (Trp^{158}), which forms part of the active site, allowed precise resolution and characterization of practically all key enzymatic steps. These steps include (i) a rapid, probably diffusion-limited substrate binding, (ii) a subsequent substrate-induced structural change (isomerization) required for the formation of the catalytically competent conformation, (iii) the rate-limiting hydrolysis step, and (iv) rapid, nonordered release of the hydrolysis products (Fig. 6*B* and Table 2). The second isomerization step was not foreseen or suggested earlier due to the lack of conformationally sensitive assays to follow the reaction. Importantly, in the present work, two independent lines of evidence argue in favor of the existence of this isomerization step. First, the different extent of quenching and blue shift associated with the enzyme-dUPNPP and enzyme-dUTP (steady-state) complexes (*cf.* Fig. 1*A*) indicate the existence of at least two distinct prehydrolysis conformations of the active site. Second, the kinetic analysis of time courses in Figs. 3, *A* and *B*, and 6 clearly shows the presence of a second slower exponential component following the initial fast binding of dUTP. An intriguing feature of the mechanism is that two different dUTP-bound intermediates will be significantly populated during steady-state dUTP hydrolysis (*E*·$dUTP^{\dagger\dagger\dagger}$ will be predominant, but about 30% of the enzyme molecules will populate *E*·$dUTP^{\dagger\dagger}$). This steady-state distribution results from the k_{ISO} rate constant being in the same order of magnitude as the rate-limiting hydrolysis rate constant (k_H) (Fig. 6*B*).

We confirmed the rate-limiting nature of the chemical (hydrolysis) step by [γ-^{32}P]dUTP-based quenched-flow transient kinetic analysis (Fig. 4). To obtain the commercially unavailable [γ-^{32}P]dUTP, we developed a simple synthesis method based on the ping-pong phosphate transfer mechanism of NDPK (26). The novelty in our synthesis is that isolation of the [^{32}P]NDPK intermediate and the final γ-^{32}P-labeled nucleotide product takes place in an Eppendorf tube, requires no instrumentation, and results in a radiochemical purity that is suitable for many applications. Laborious purification of the synthesis products is not necessary, because the donor and acceptor nucleotides are spatially and temporally separated.

This straightforward method may be of great help in studying enzymes that use pyrimidine-triphosphates as substrate (*e.g.* dCTP deaminase, dTTPase, tRNA cytidyltransferase, etc.), since none of these relevant γ-labeled pyrimidine nucleotides are commercially available (or they may be purchased only as expensive custom synthesis orders). Due to the substrate promiscuity of NDPK, even base-modified nucleotide analogs may be radioactively labeled using this method for additional specific applications.

Interestingly, the estimated intracellular dUTP concentration (~0.7 μM (4)) is in the same range as the K_M of hDUT for dUTP (Tables 1 and 2). This indicates that dUTPase function is highly sensitive to cellular dUTP fluctuations around the physiological level. Our data show that product inhibition by dUMP at its estimated physiological concentration (~2.7 μM (4)) is probably not significant due to its relatively low affinity for hDUT and its rapid release from the enzyme-products complex (Tables 1 and 2).

We probed *in silico* F158W mutations in available structures and found that the replacement of Phe^{158} with a Trp residue does not cause a steric hindrance within the active site. Accordingly, we found that $hDUT^{W158}$ retains the enzymatic activity of the wild-type enzyme. The presence of an aromatic residue at this location has been suggested to be important for enzyme activity (12), and thus the fact that a Trp residue can functionally replace the native Phe^{158} implies that the fluorescence signal reports events that are highly relevant to the physiological activity of the enzyme.

Trp^{158} is sensitive to the precise nucleotide (or other ligand) content of the active site (Fig. 1*A*). The solvent shielding of Trp^{158} increases, whereas the structural flexibility of this residue decreases with increasing length of the polyphosphate chain of the nucleotide ligand (Fig. 2). PP_i binding into the binding site, however, causes a structural ordering of the arm without a solvent shielding effect. Based on our observation that $E{\cdot}PP_i$ exhibits elevated fluorescence compared with the apoenzyme (Fig. 1*A*), we speculate that PP_i binding may cause disruption of a quenching interaction of Trp^{158}, supposed to be present in the apo state. A possibility for such a quenching interaction is a cation-π type interaction (33) between Trp^{158} and the positively charged guanidino moiety of an arginine residing in its close proximity. Candidate arginines are residues 85, 128, and 135, all contributing to the binding and stabilization of the polyphosphate chain of the substrate nucleotide (Fig. 7) (13). These groups are separated by about 9–10 Å from Trp^{158} via the intercalation of the uracil group in the hDUT-dUPNPP structure. In the apo state, however, one of the candidate arginines might move closer to the phenylalanine (tryptophan) to neutralize the positive charge via cation-π stacking; hence the intermediate fluorescence level observed in the $apo\text{-}hDUT^{W158}$.

It is noteworthy that, whereas the binding of dUMP, dUDP, and dUPNPP (and even more that of dUTP) to the enzyme causes marked quenching of Trp^{158} as compared with the apo state, the posthydrolysis $E{\cdot}dUMP{\cdot}PP_i$ complex has an enhanced Trp^{158} fluorescence. We surmise that this fluorescence increase reflects a structural state in which the stacking interaction between Trp^{158} and the uracil moiety is at least partially disrupted, aiding the rapid release of products from this posthydrolytic complex.

In addition to its utility in the determination of the kinetic and thermodynamic parameters, the Trp^{158} signal also provided much information about the structural dynamics of the C-terminal arm during catalysis. Evidence is presented that this protein segment is at least partially closed upon the active site in all enzymatic states (even including the apoenzyme) (Fig. 2), and therefore its conformational freedom may be well restricted. Fig. 7 shows that the C-terminal arm of monomer A is anchored in a β-sheet with the N-terminal residues of monomer C. At its very C terminus, the arm also interacts with monomer B via strong hydrogen bonds (second anchor). Interactions of the arm with the ligand dUPNPP are mainly formed by residues situated between the monomer-monomer interacting regions. This arrangement rationalizes (i) the proposed proximity of the C terminus to the protein core even in the absence of nucleotide (in the apoenzyme) and (ii) that the C-terminal arm still conveys a significant flexibility in the apoenzyme (between the two anchor regions), as suggested in previous studies (12, 13).

We described a complex methodology to assess the fundamental steps of dUTP hydrolysis as catalyzed by human dUTPase, an important chemotherapeutic target protein. The resulting novel insights underline the importance of the dynamic behavior of the C-terminal arm during catalysis and advocate the targeting of this enzyme segment for perturbation of dUTPase function.

Acknowledgments—We thank Dr. Orsolya Barabás for useful comments on the manuscript and the Department of Immunology of Eötvös Loránd University, Budapest, for use of scintillation counter equipment.

REFERENCES

1. Shlomai, J., and Kornberg, A. (1978) *J. Biol. Chem.* **253,** 3305–3312
2. Gadsden, M. H., McIntosh, E. M., Game, J. C., Wilson, P. J., and Haynes, R. H. (1993) *EMBO J.* **12,** 4425–4431
3. el-Hajj, H. H., Zhang, H., and Weiss, B. (1988) *J. Bacteriol.* **170,** 1069–1075
4. Traut, T. W. (1994) *Mol. Cell Biochem.* **140,** 1–22
5. Pearl, L. H., and Savva, R. (1996) *Nat. Struct. Biol.* **3,** 485–487
6. Pugacheva, E. N., Ivanov, A. V., Kravchenko, J. E., Kopnin, B. P., Levine, A. J., and Chumakov, P. M. (2002) *Oncogene* **21,** 4595–4600
7. Chano, T., Mori, K., Scotlandi, K., Benini, S., Lapucci, C., Manara, M. C., Serra, M., Picci, P., Okabe, H., and Baldini, N. (2004) *Oncol. Rep.* **11,** 1257–1263
8. Ladner, R. D., Lynch, F. J., Groshen, S., Xiong, Y. P., Sherrod, A., Caradonna, S. J., Stoehlmacher, J., and Lenz, H. J. (2000) *Cancer Res.* **60,** 3493–3503
9. Romeike, B. F., Bockeler, A., Kremmer, E., Sommer, P., Krick, C., and Grasser, F. (2005) *Pathol. Res. Pract.* **201,** 727–732
10. Strahler, J. R., Zhu, X. X., Hora, N., Wang, Y. K., Andrews, P. C., Roseman, N. A., Neel, J. V., Turka, L., and Hanash, S. M. (1993) *Proc. Natl. Acad. Sci. U. S. A.* **90,** 4991–4995
11. Bekesi, A., Zagyva, I., Hunyadi-Gulyas, E., Pongracz, V., Kovari, J., Nagy, A. O., Erdei, A., Medzihradszky, K. F., and Vertessy, B. G. (2004) *J. Biol. Chem.* **279,** 22362–22370
12. Mol, C. D., Harris, J. M., McIntosh, E. M., and Tainer, J. A. (1996) *Structure* **4,** 1077–1092
13. Varga, B., Barabás, O., Kovári, J., Tóth, J., Hunyadi-Gulyás, É., Klement, É., Medzihradszky, K. F., Tölgyesi, F., Fidy, J., and Vertessy, B. G. (2007) *FEBS*

Lett. **581,** 4783–4788
14. Larsson, G., Svensson, L. A., and Nyman, P. O. (1996) *Nat. Struct. Biol.* **3,** 532–538
15. Prasad, G. S., Stura, E. A., Elder, J. H., and Stout, C. D. (2000) *Acta Crystallogr Sect. D. Biol. Crystallogr.* **56,** 1100–1109
16. Barabas, O., Pongracz, V., Kovari, J., Wilmanns, M., and Vertessy, B. G. (2004) *J. Biol. Chem.* **279,** 42907–42915
17. Nemeth-Pongracz, V., Barabas, O., Fuxreiter, M., Simon, I., Pichova, I., Rumlova, M., Zabranska, H., Svergun, D., Petoukhov, M., Harmat, V., Klement, E., Hunyadi-Gulyas, E., Medzihradszky, K. F., Konya, E., and Vertessy, B. G. (2007) *Nucleic Acids Res.* **35,** 495–505
18. Dauter, Z., Persson, R., Rosengren, A. M., Nyman, P. O., Wilson, K. S., and Cedergren-Zeppezauer, E. S. (1999) *J. Mol. Biol.* **285,** 655–673
19. Vertessy, B. G., Larsson, G., Persson, T., Bergman, A. C., Persson, R., and Nyman, P. O. (1998) *FEBS Lett.* **421,** 83–88
20. Vertessy, B. G. (1997) *Proteins* **28,** 568–579
21. Larsson, G., Nyman, P. O., and Kvassman, J. O. (1996) *J. Biol. Chem.* **271,** 24010–24016
22. Kovári, J., Barabás, O., Varga, B., Békési, A., Tölgyesi, F., Fidy, J., Nagy, J., and Vertessy, B. G. (2007) *Proteins*, in press
23. Margossian, S. S., and Lowey, S. (1982) *Methods Enzymol.* **85,** 55–71
24. Mendes, P. (1997) *Trends Biochem. Sci.* **22,** 361–363
25. Lakowicz, J. (1999) *Principles of Fluorescence Spectroscopy*, 2nd Ed., pp. 291–306 and 237–251, Springer-Verlag New York Inc., New York
26. Munoz-Dorado, J., Inouye, S., and Inouye, M. (1990) *J. Biol. Chem.* **265,** 2707–2712
27. Sambrook, J., and Russell, D. W. (2001) *Molecular Cloning: A Laboratory Manual*, Cold Spring Harbor Laboratory, Cold Spring Harbor, NY
28. Li, X. D., Rhodes, T. E., Ikebe, R., Kambara, T., White, H. D., and Ikebe, M. (1998) *J. Biol. Chem.* **273,** 27404–27411
29. Kovacs, M., Malnasi-Csizmadia, A., Woolley, R. J., and Bagshaw, C. R. (2002) *J. Biol. Chem.* **277,** 28459–28467
30. Lascu, I., and Gonin, P. (2000) *J. Bioenerg. Biomembr.* **32,** 237–246
31. White, H. D., Belknap, B., and Webb, M. R. (1997) *Biochemistry* **36,** 11828–11836
32. Molnar, J., and Lorand, L. (1961) *Arch. Biochem. Biophys.* **93,** 353–363
33. Gallivan, J. P., and Dougherty, D. A. (1999) *Proc. Natl. Acad. Sci. U. S. A.* **96,** 9459–9464